

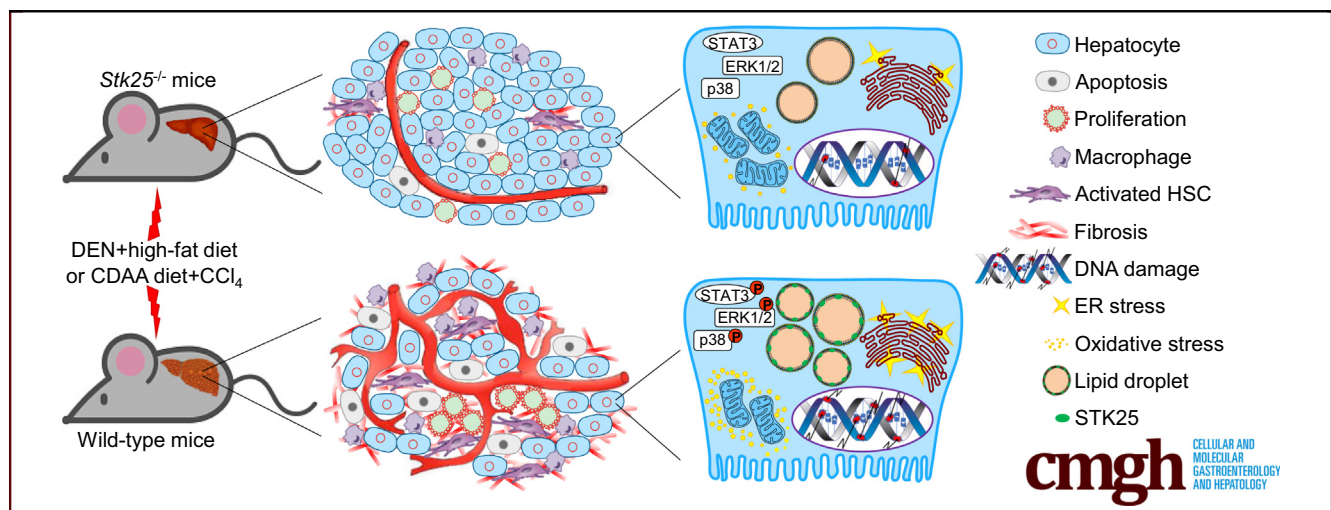
ORIGINAL RESEARCH

Antagonizing STK25 Signaling Suppresses the Development of Hepatocellular Carcinoma Through Targeting Metabolic, Inflammatory, and Pro-Oncogenic Pathways



Yeshwant Kurhe,¹ Mara Caputo,¹ Emmelie Cansby,¹ Ying Xia,¹ Sima Kumari,¹ Sumit Kumar Anand,¹ Brian W. Howell,² Hanns-Ulrich Marschall,³ and Margit Mahlapuu¹

¹Department of Chemistry and Molecular Biology, ³Department of Molecular and Clinical Medicine, Wallenberg Laboratory, Institute of Medicine, University of Gothenburg and Sahlgrenska University Hospital, Gothenburg, Sweden; ²Department of Neuroscience and Physiology, State University of New York Upstate Medical University, Syracuse, New York



SUMMARY

We provide evidence that antagonizing STK25 activity hinders the development of hepatocellular carcinoma, which is one of the most fatal cancers. This study provides an impetus for further analysis of STK25 as a therapeutic target in liver cancer.

BACKGROUND & AIMS: Hepatocellular carcinoma (HCC) is one of the most fatal and fastest-growing cancers. Recently, nonalcoholic steatohepatitis (NASH) has been recognized as a major catalyst for HCC. Thus, additional research is critically needed to identify mechanisms involved in NASH-induced hepatocarcinogenesis, to advance the prevention and treatment of NASH-driven HCC. Because the sterile 20-type kinase serine/threonine kinase 25 (STK25) exacerbates NASH-related phenotypes, we investigated its role in HCC development and aggravation in this study.

METHODS: Hepatocarcinogenesis was induced in the context of NASH in *Stk25* knockout and wild-type mice by combining chemical procarcinogens and a dietary challenge. In the first cohort, a single injection of diethylnitrosamine was combined with a high-fat diet-feeding. In the second cohort, chronic

administration of carbon tetrachloride was combined with a choline-deficient L-amino-acid-defined diet. To study the cell-autonomous mode of action of STK25, we silenced this target in the human hepatocarcinoma cell line HepG2 by small interfering RNA.

RESULTS: In both mouse models of NASH-driven HCC, the livers from *Stk25*^{-/-} mice showed a markedly lower tumor burden compared with wild-type controls. We also found that genetic depletion of STK25 in mice suppressed liver tumor growth through reduced hepatocellular apoptosis and decreased compensatory proliferation, by a mechanism that involves protection against hepatic lipotoxicity and inactivation of STAT3, ERK1/2, and p38 signaling. Consistently, silencing of STK25 suppressed proliferation, apoptosis, migration, and invasion in HepG2 cells, which was accompanied by lower expression of the markers of epithelial-mesenchymal transition and autophagy flux.

CONCLUSIONS: This study provides evidence that antagonizing STK25 signaling hinders the development of NASH-related HCC and provides an impetus for further analysis of STK25 as a therapeutic target for NASH-induced HCC treatment in human beings. (*Cell Mol Gastroenterol Hepatol* 2022;13:405-423; <https://doi.org/10.1016/j.jcmgh.2021.09.018>)

Keywords: STK25; Hepatocellular Carcinoma; NASH; CDAA; DEN.

Worldwide, liver cancer is the sixth most common cancer and the second leading cause of cancer-related deaths (approximately 800,000 per year, a figure that is increasing).¹ Hepatocellular carcinoma (HCC) constitutes approximately 90% of primary liver cancers and is refractory to nearly all currently available anticancer therapies.¹ The well-known risk factors for HCC are hepatitis B and C virus infections and alcohol abuse. Recently, attention has focused on the importance of nonalcoholic steatohepatitis (NASH) in the development of HCC. First report linking NASH to HCC appeared in 2001,² and, to date, NASH has been reported in several studies as the single most common and rapidly increasing underlying etiology of HCC.^{3–5}

NASH is a severe stage of nonalcoholic fatty liver disease (NAFLD) and is characterized by hepatic lipid accumulation (ie, steatosis), meta-inflammation, and cellular damage (hallmarked by hepatocyte ballooning) with different stages of local fibrosis.^{6,7} The prevalence of NASH is increasing rapidly because of the pandemic spread of obesity, which is the main risk factor of NAFLD/NASH.⁴ The HCC incidence among NASH patients can vary from 2.4% to 12.8%⁸; however, the nature of the signals that underpin the aggravation of NASH into HCC remains elusive and it is not known why some NASH patients rapidly progress to HCC while others do not. Importantly, compared with HCC triggered by viral infection or alcohol, NASH-related HCC is reportedly less likely to be detected at surveillance and more likely to be treated less effectively.^{9,10} Thus, there is a strong medical need for new predictors and improved treatments of NASH-driven HCC.

Our recent translational studies have identified the liver lipid droplet-decorating protein kinase serine/threonine kinase 25 (STK25, also referred to as YSK1 or SOK1) as a new regulator of hepatic lipid partitioning.^{11–17} Furthermore, we found that STK25 critically controls liver meta-inflammation, oxidative and endoplasmic reticulum (ER) stress, as well as the autophagic degradation system,^{12–17} which all have been described as key factors leading to HCC development in the context of NASH.^{8,18,19} On the basis of this evidence, we now hypothesize that STK25 is an important mediator in the complex and integrated molecular network driving the initiation and progression of NASH-related HCC, and a potential target for anti-HCC therapy.

To decipher the possible role of STK25 in NASH-driven HCC, we here used the *Stk25*^{-/-} mouse model, in which hepatocarcinogenesis was induced in the context of NASH by combining chemical procarcinogens and a dietary challenge. In the first cohort of *Stk25*^{-/-} mice and wild-type littermates, HCC was triggered by a single injection of diethylnitrosamine (DEN), which is known to alkylate DNA and promote oxidative stress via the production of reactive oxygen species (ROS),^{20,21} combined with long-term high-fat diet-feeding to induce hepatic steatosis, inflammation, and fibrosis (ie, the spectrum of lesions present in NASH patients). In the second cohort of mice, the choline-deficient

L-amino-acid-defined (CDAA) diet was used to produce liver steatosis, meta-inflammation, and nutritional fibrosis,^{22–24} and this dietary regimen was combined with chronic low-dose administration of carbon tetrachloride (CCl₄), a toxin that accelerates extracellular matrix deposition and necrosis in the liver through its metabolite CCl₃.^{25,26} Our study identifies STK25 signaling as a critical driver of the initiation and progression of HCC by showing that genetic ablation of STK25 efficiently suppressed tumor development in 2 mouse models of hepatocarcinogenesis that closely recapitulated the nature of human HCC.

Results

Genetic Ablation of STK25 Hinders the Development of HCC in Mice

We used the *Stk25*^{-/-} mouse model, which has a germline ablation of STK25,²⁷ to test the hypothesis that STK25 contributes to the initiation and aggravation of DEN-induced HCC during overnutrition (Figure 1A). We found that all DEN-injected wild-type mice, following high-fat diet-feeding for 30 weeks, developed numerous macroscopic nodules of variable size in the liver (Figure 1B). Interestingly, we observed that the maximal and total volume of visible HCC tumors was reduced by 2.9- ± 0.5-fold and 3.7- ± 0.5-fold, respectively, by the loss of STK25 in knockout mice compared with their wild-type littermates (Figure 1C). Furthermore, there was a tendency for lower numbers of surface HCC tumors in *Stk25*^{-/-} livers (Figure 1C). Together, these results suggest that both tumor initiation and growth were affected by STK25 ablation. Consistent with these morphologic investigations in whole-liver samples, we found less-extensive damage in H&E-stained liver sections from *Stk25*^{-/-} vs wild-type mice, associated with a significantly reduced labeling for HCC markers α -fetoprotein (AFP) and Yes-associated protein (YAP) (Figure 1D and E).^{28,29} Furthermore, immunohistologic assessment indicated that tumors from wild-type mice expressed higher levels of glucose regulatory protein 78 (GRP78) and epithelial cell adhesion molecule (EpcAM), whose abundance is known to correlate with HCC grade and poor patient prognosis (Figure 2A).³⁰

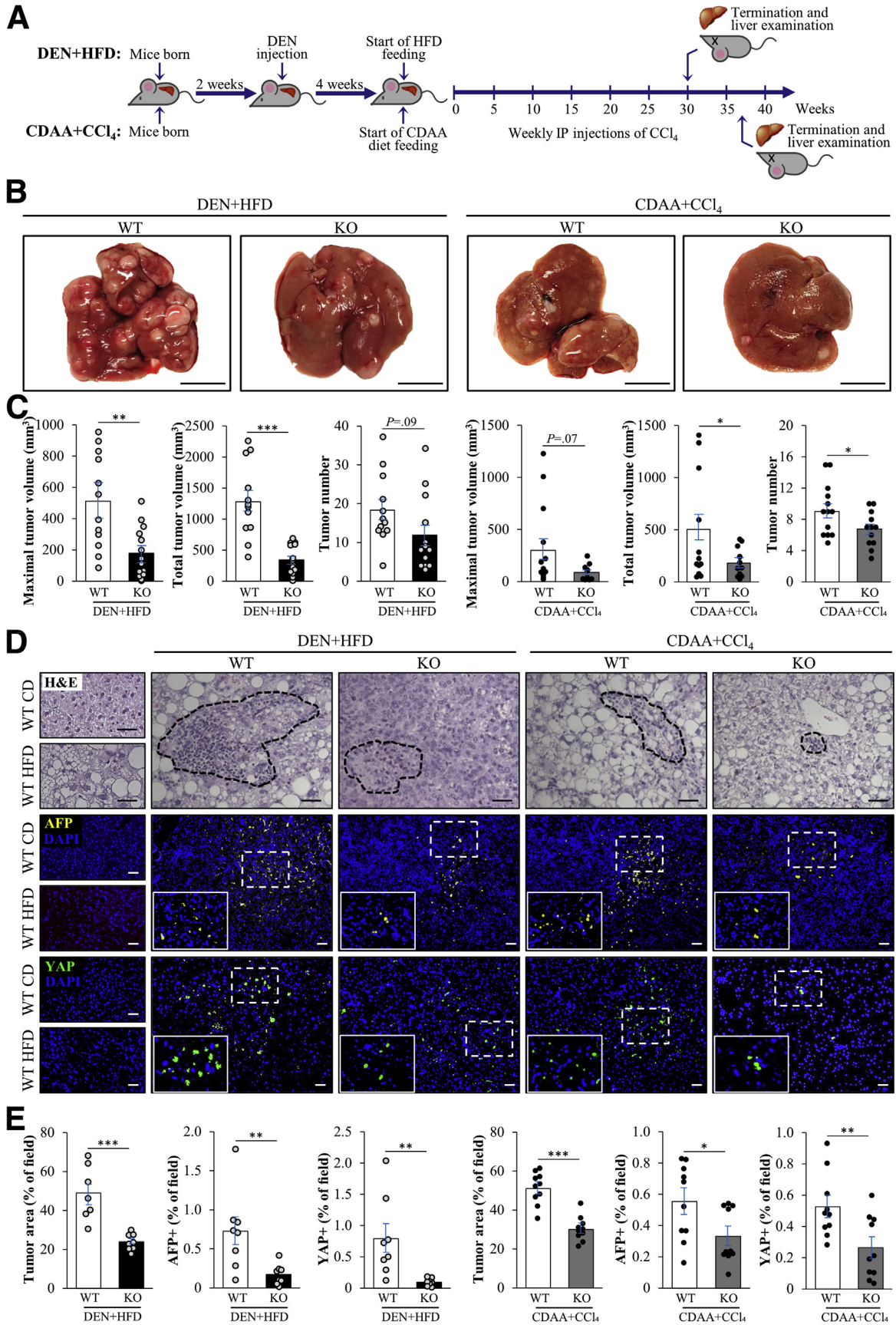
Abbreviations used in this paper: AFP, α -fetoprotein; BrdU, bromodeoxyuridine; CASP3, caspase 3; CDAA, choline-deficient L-amino-acid-defined; DEN, diethylnitrosamine; EMT, epithelial-mesenchymal transition; EpcAM, epithelial cell adhesion molecule; ER, endoplasmic reticulum; ERK, extracellular signal-regulated kinase; GRP78, glucose regulatory protein 78; HCC, hepatocellular carcinoma; JNK, Jun N-terminal kinase; MST, mammalian sterile 20-like; NAFLD, non-alcoholic fatty liver disease; NASH, nonalcoholic steatohepatitis; PCNA, proliferating cell nuclear antigen; ROS, reactive oxygen species; siRNA, small interfering RNA; STAT3, signal transducer and activator of transcription 3; STK25, serine/threonine kinase 25; YAP, Yes-associated protein.

 Most current article

© 2021 The Authors. Published by Elsevier Inc. on behalf of the AGA Institute. This is an open access article under the CC BY license (<https://creativecommons.org/licenses/by/4.0/>).

2352-345X

<https://doi.org/10.1016/j.jcmgh.2021.09.018>



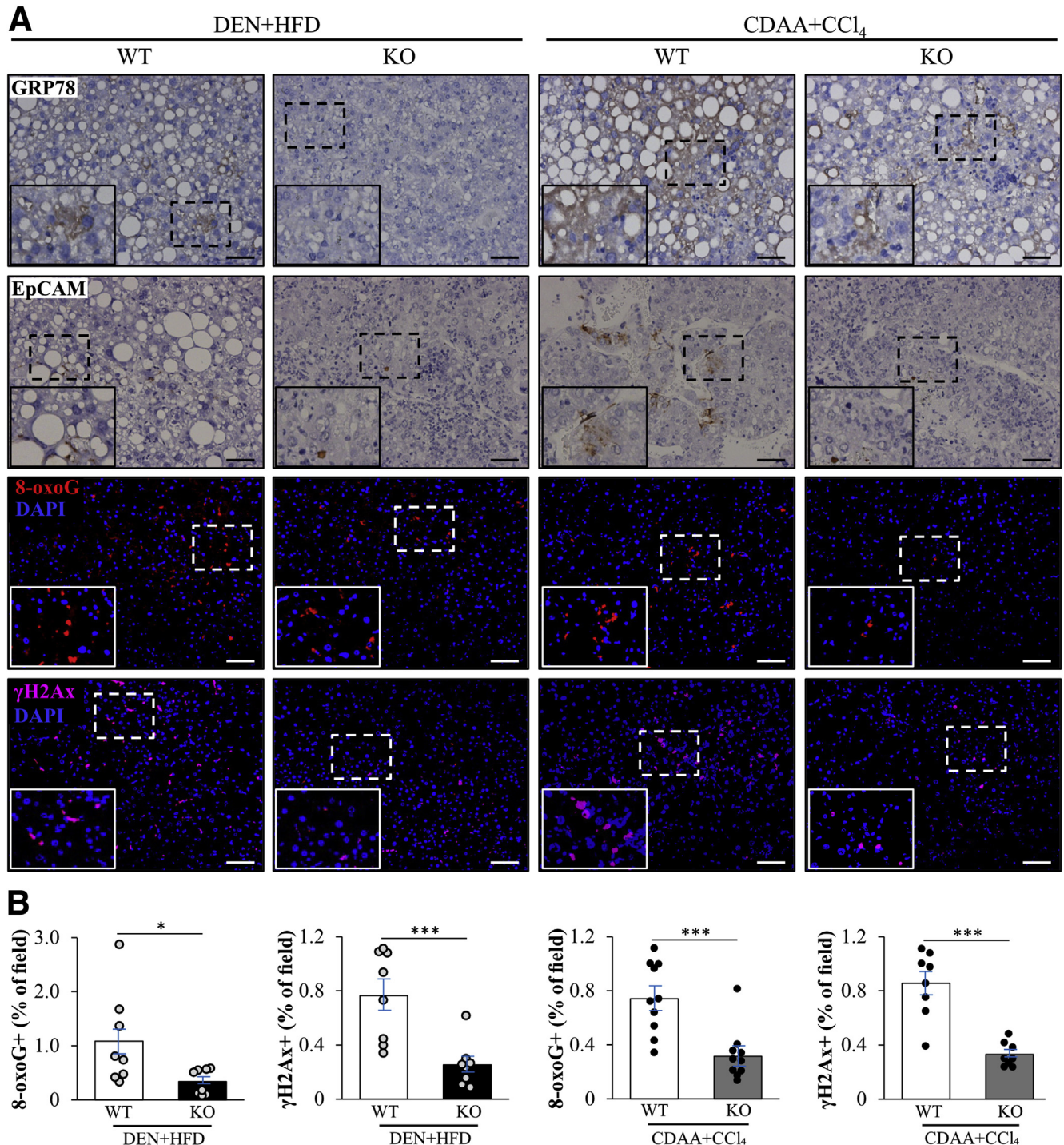
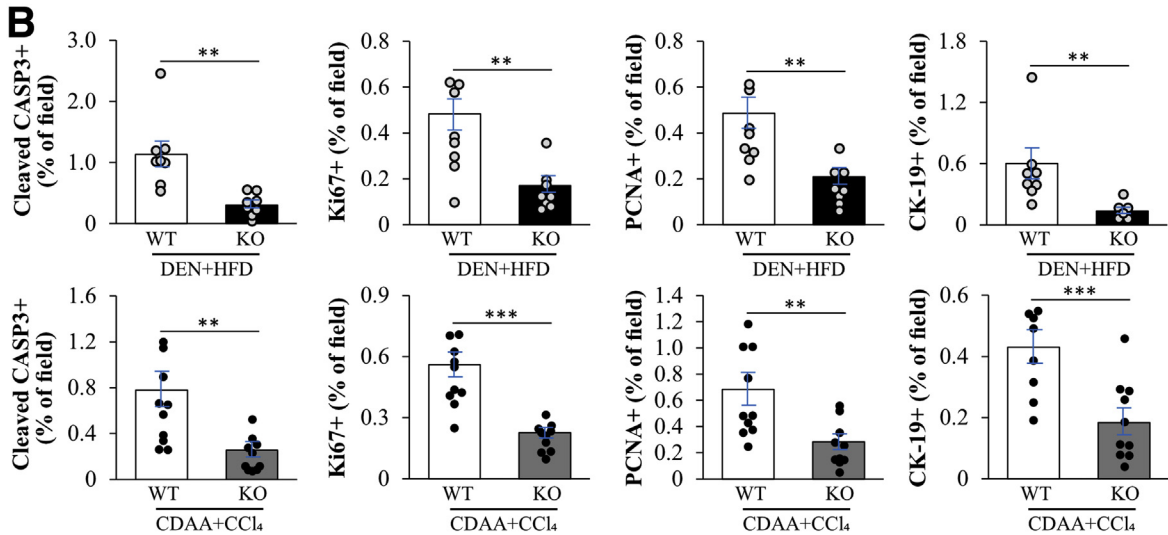
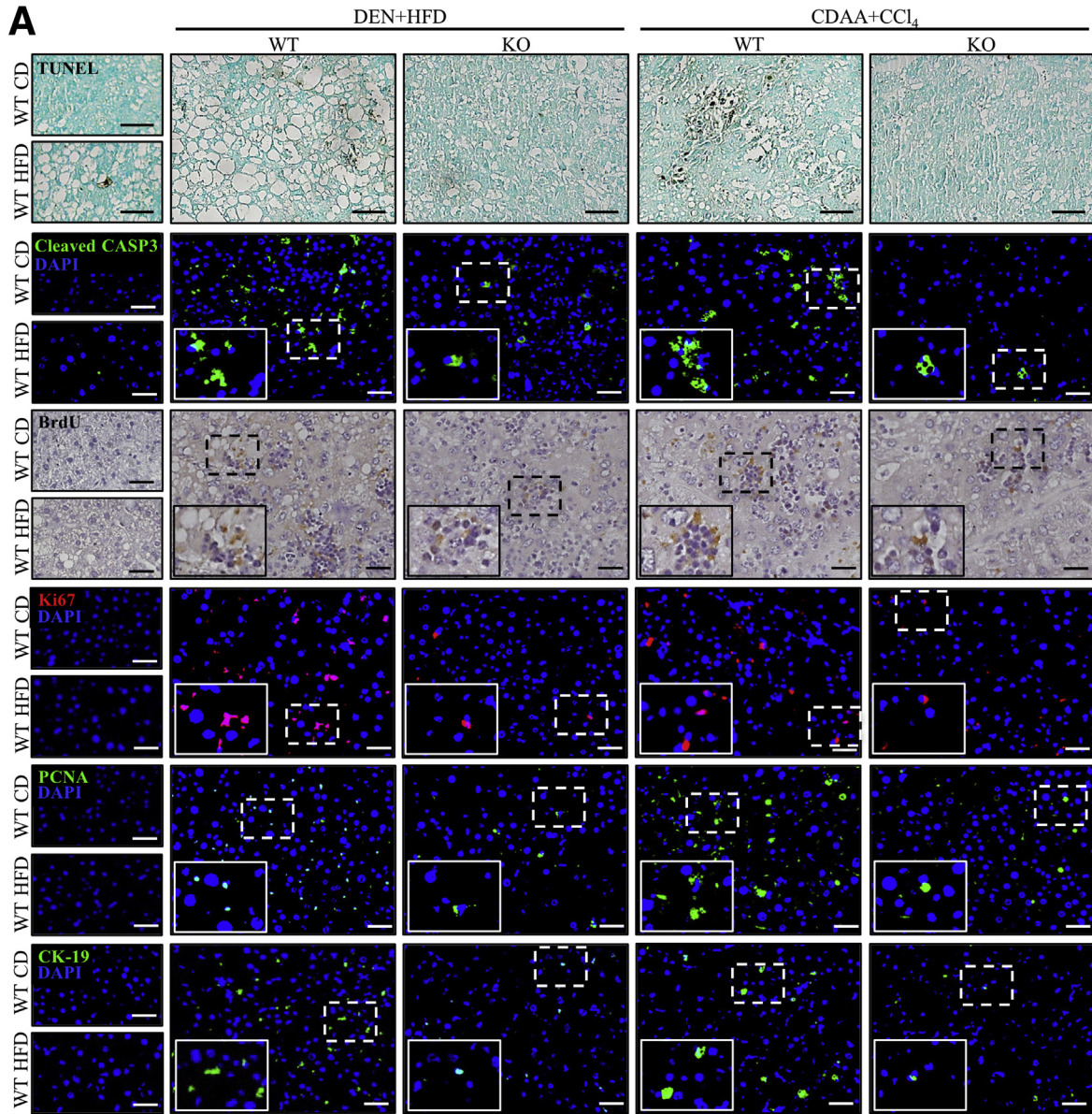


Figure 2. Knockout of STK25 in mice with DEN- or CDAA-induced HCC suppresses GRP78 and EpCAM abundance and reduces DNA damage. (A) Representative liver sections processed for immunohistochemistry/immunofluorescence with anti-GRP78 (brown), anti-EpCAM (brown), anti-8-oxoguanine (red), or anti-γH2Ax (pink) antibodies; counterstaining with hematoxylin in immunohistochemistry images; nuclei stained with DAPI (blue) in immunofluorescence images. (B) Quantification of the immunofluorescence staining. Scale bars: 50 μm. Data are means ± SEM from 8 to 10 mice per group. DAPI, 4',6-diamidino-2-phenylindole; HFD, high-fat diet; KO, knockout; WT, wild-type. **P* < .05, ****P* < .001.

Figure 1. (See previous page). Genetic ablation of STK25 suppresses tumor development in DEN- or CDAA-induced hepatocarcinogenesis models in mice. (A) Schematic presentation of the experimental design of the in vivo studies. (B) Representative images of whole liver. Scale bars: 1 cm. (C) Quantification of tumor volume and number. (D) Representative liver sections stained with H&E or processed for immunofluorescence with anti-AFP (yellow) or anti-YAP (green) antibodies; nuclei stained with DAPI (blue). Scale bars: 50 μm. (E) Quantification of the tumor area and immunofluorescence staining. Data are means ± SEM from 8 to 14 mice per group. CD, chow diet; DAPI, 4',6-diamidino-2-phenylindole; HFD, high-fat diet; IP, intraperitoneal; KO, knockout; WT, wild-type. **P* < .05, ***P* < .01, and ****P* < .001.



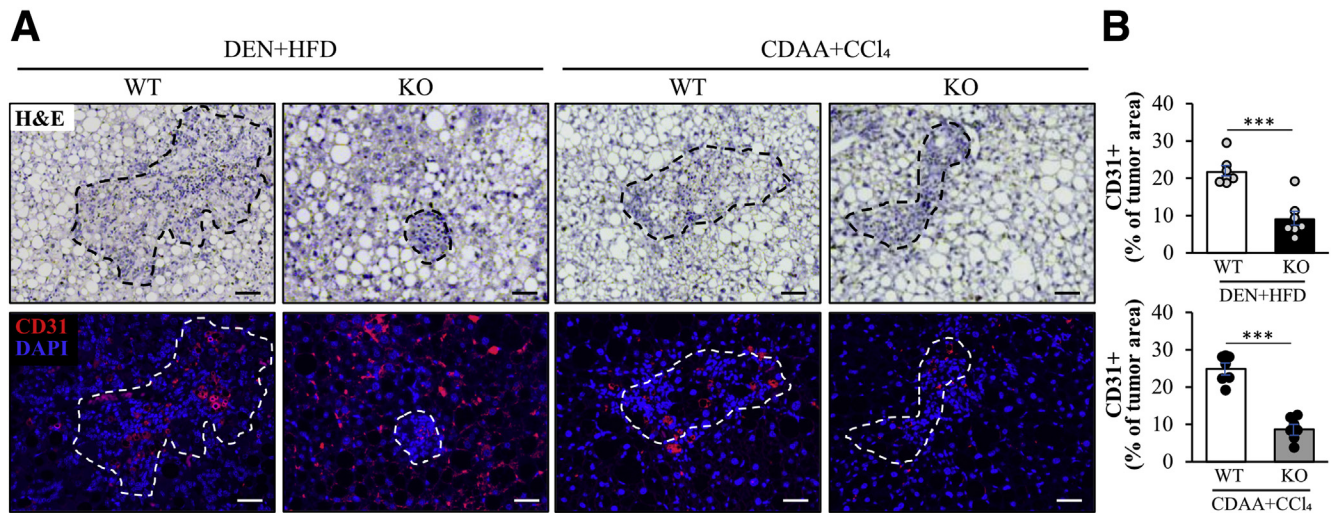


Figure 4. Knockout of STK25 reduces tumor angiogenesis in mouse models of DEN- or CDAA-induced HCC. (A) Representative liver sections stained with H&E or processed for immunofluorescence with anti-CD31 (red) antibody; nuclei stained with DAPI (blue) in immunofluorescence images. (B) Staining with anti-CD31 antibody was selectively quantified in tumor tissue identified from the H&E staining on a serial section (shown by dashed lines). Scale bars: 50 μ m. Data are means \pm SEM from 7 mice per group. DAPI, 4',6-diamidino-2-phenylindole; HFD, high-fat diet; KO, knockout; WT, wild-type. *** $P < .001$.

We also compared CDAA diet-induced HCC carcinogenesis in *Stk25*^{-/-} and wild-type mice (Figure 1A). We observed that all wild-type mice fed a CDAA diet and injected with a low dose of CCl₄ for 37 weeks developed numerous visible tumors in the liver (Figure 1B). In agreement with the DEN-induced HCC model, the tumor load was reduced in livers from *Stk25*^{-/-} vs wild-type mice, including a decrease in the maximal and total volume as well as the number of macroscopic HCC nodules (Figure 1C). Furthermore, we detected a significantly smaller region with cellular damage in H&E-stained liver sections from *Stk25*^{-/-} vs wild-type mice along with reduced immunostaining for AFP, YAP, GRP78, and EpCAM (Figures 1D and E and 2A).

Together, these 2 translational models of HCC highlight STK25 as a critical regulator of hepatocarcinogenesis.

STK25 Abrogation Alleviates HCC Through Suppressed Hepatocyte Proliferation and Decreased Angiogenesis

To explore the mechanisms by which a depletion of STK25 exerts a tumor-mitigating effect, we first examined whether the loss of STK25 decreased the susceptibility of knockout mice to hepatocarcinogenesis by augmenting cell death. On the contrary, we observed significantly reduced apoptosis in the livers from *Stk25*^{-/-} mice compared with wild-type controls, as shown by less terminal

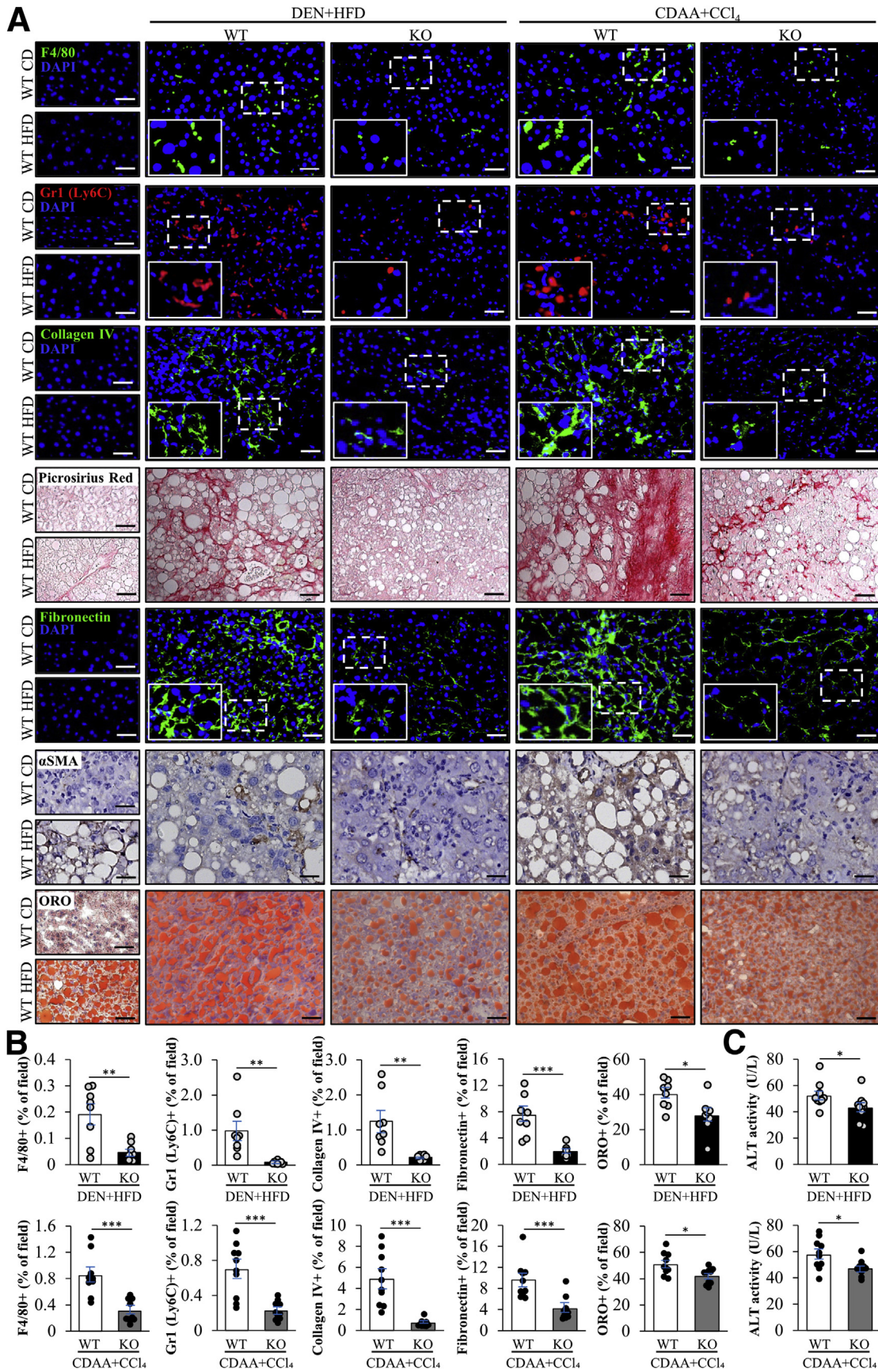
deoxynucleotidyl transferase-mediated deoxyuridine triphosphate nick-end labeling (TUNEL)—as well as cleaved caspase 3 (CASP3)-positive cells. This applied both to DEN- and CDAA-induced models of HCC (Figure 3).

It has been shown previously that hepatocyte apoptosis stimulates the compensatory proliferation in liver tissue that in turn promotes carcinogenesis in HCC.³¹⁻³⁴ Based on this evidence, we next examined whether STK25 deficiency also suppresses the proliferation of hepatocytes. Indeed, we detected less bromodeoxyuridine (BrdU)-positive cells in the livers from *Stk25*^{-/-} mice than in wild-type mice (Figure 3A). Consistently, 3 independent methods of evaluating hepatocyte proliferation—immunostaining for proliferation markers Ki67, proliferating cell nuclear antigen (PCNA), and cytokeratin-19—all showed significantly decreased numbers of proliferating cells in the livers from *Stk25*^{-/-} mice as opposed to wild-type controls (Figure 3), and this difference was observed both in DEN- and CDAA-induced models of HCC.

Tumor angiogenesis is an important driver of hepatocellular tumor growth.^{35,36} We therefore investigated tumor vascularization by immunostaining of liver sections with an anti-CD31 antibody. In both models of HCC, we found a significant reduction in vessel density in tumors from *Stk25* knockout mice compared with their wild-type littermates (Figure 4).

Together, these data suggest that STK25 abrogation confers resistance to hepatocyte apoptosis induced by DEN

Figure 3. (See previous page). STK25 deficiency attenuates apoptosis and proliferation in mouse models of DEN- or CDAA-induced HCC. (A) Representative liver sections stained with terminal deoxynucleotidyl transferase-mediated deoxyuridine triphosphate nick-end labeling (TUNEL) or processed for immunohistochemistry/immunofluorescence with anti-cleaved CASP3 (green), anti-BrdU (brown), anti-Ki67 (red), anti-PCNA (green), or anti-cytokeratin-19 (anti-CK-19) (green) antibodies; counterstaining with methyl green (TUNEL) or hematoxylin (BrdU); nuclei stained with DAPI (blue) in immunofluorescence images. (B) Quantification of the staining. Scale bars: 50 μ m. Data are means \pm SEM from 8 to 10 mice per group. CD, chow diet; DAPI, 4',6-diamidino-2-phenylindole; HFD, high-fat diet; KO, knockout; WT, wild-type. ** $P < .01$, *** $P < .001$.



or CDAA challenge, and suppresses HCC development through attenuated tumor cell proliferation and angiogenesis.

STK25 Deficiency Protects HCC-Bearing Mice Against Diet-Induced Liver Steatosis, Meta-Inflammation, and Fibrosis

Compensatory proliferation after liver damage has been suggested to be triggered by hepatic inflammation mediated primarily by macrophages.^{28,31,32} Hepatic macrophages can arise either from circulating bone marrow-derived monocytic precursors or from self-renewing embryo-derived local macrophages, termed *Kupffer cells*³⁷; both macrophage populations are positive for F4/80 while freshly infiltrating monocyte-derived macrophages also are characterized by high expression of Gr1 (Ly6C). Here, we found that loss of STK25 protected against hepatic macrophage infiltration in both DEN- and CDAA-induced models of HCC as evidenced by a lower number of F4/80- and Gr1 (Ly6C)-positive cells in the liver sections from *Stk25*^{-/-} vs wild-type mice (Figure 5A and B). Furthermore, HCC-bearing *Stk25* knockout mice had reduced hepatic fibrosis as shown by reduced staining for collagen IV, Picrosirius Red (stains both collagen type I and type III), and fibronectin (Figure 5A and B). Consistently, immunostaining for α smooth muscle actin (α SMA), a marker for activated hepatic stellate cells, was lower in liver sections from *Stk25*^{-/-} mice (Figure 5A). Diet-induced lipid accumulation in hepatocytes also was mitigated by STK25 abrogation in both models of HCC as shown by a smaller area stained with Oil Red O, which labels neutral lipids (Figure 5A and B). The improvement in histopathology correlated with lower plasma alanine transaminase (ALT) levels in *Stk25*^{-/-} vs wild-type mice (Figure 5C).

Together, in addition to inhibition of liver tumorigenesis, loss of STK25 in both HCC models substantially suppressed all the pathologic features of NASH, including hepatic steatosis, inflammation, and fibrosis.

Genetic Ablation of STK25 Suppresses Oxidative and ER Stress in the Liver

ER stress and accumulation of ROS within liver parenchymal cells result in compensatory proliferation of differentiated hepatocytes that are otherwise quiescent, which is one of the major pathogenic mechanisms underlying HCC development.³⁸ Indeed, we found that lower hepatocyte proliferation in HCC-bearing *Stk25* knockout mice was accompanied by reduced oxidative stress as evidenced by repressed levels of superoxide radicals ($O_2^{\bullet-}$) quantified by

dihydroethidium staining, abrogated oxidative DNA damage detected by immunostaining for 8-oxoguanine and γ H2Ax, and protection against deposition of lipid peroxidation products and oxidized phospholipids measured by immunostaining for 4-hydroxynonenal (4-HNE) and E06, respectively (Figures 2A and B and 6A and B). In parallel with these alterations in oxidative stress markers, we detected significantly reduced immunostaining for KDEL (a signal motif for ER retrieval) and C/EBP homologous protein (CHOP; a marker for ER stress-induced cell death) in the livers from *Stk25* knockout mice with both DEN- and CDAA-induced HCC (Figure 6A and B).

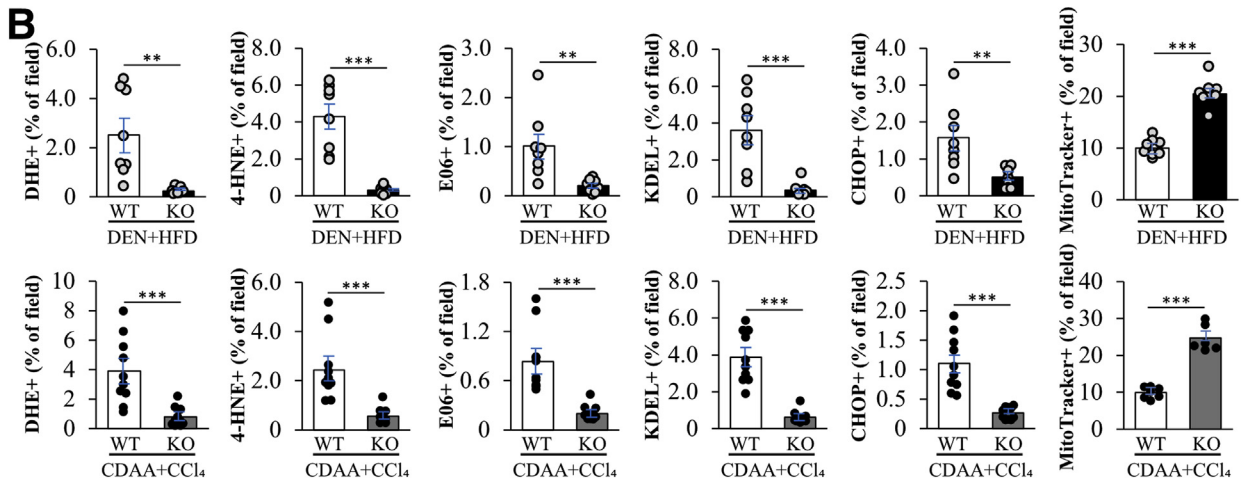
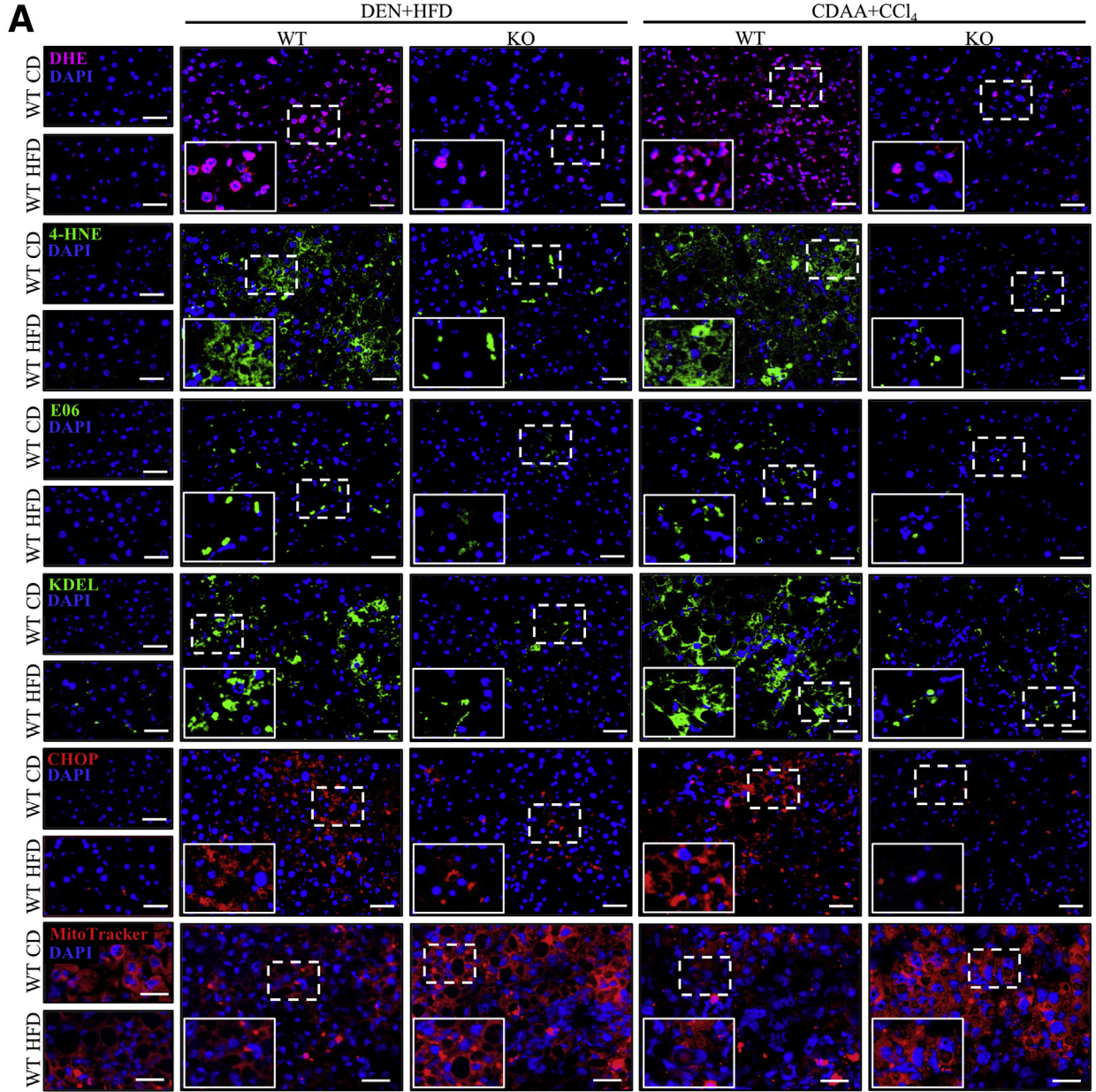
Aberrant mitochondrial activity, leading to heightened ROS production, is known to be associated with liver tumorigenesis.^{39,40} Consistent with higher oxidative stress, we found that mitochondrial activity was approximately 2-fold lower in the livers from wild-type mice compared with *Stk25*^{-/-} mice (Figure 6A and B).

STK25 Disruption Reduces ERK1/2, p38, and STAT3 Signaling in the DEN-Induced HCC Model

To explore the mechanisms by which STK25 depletion protects against hepatocellular carcinogenesis, we performed immunoblot analysis in the liver tumors isolated from mice with DEN-induced HCC to monitor the hepatic activation status of mitogen-activated protein kinases (MAPKs) extracellular signal-regulated kinase 1/2 (ERK1/2), Jun N-terminal kinase (JNK), and p38, which are important signaling components controlling proliferation, differentiation, and migration in HCC.⁴¹ We observed higher phosphorylation levels of ERK1/2 as well as p38 MAPK, shown to be activated in the majority of human HCCs,^{30,42-44} in the liver tumors from wild-type vs *Stk25*^{-/-} mice (Figure 7A and C). Notably, hepatic JNK activation, known to be required for DEN-induced HCC in mice,⁴⁵ was not altered by depletion of STK25 (Figure 7B).

It recently was shown that the inactivation of negative regulators of signal transducer and activator of transcription 3 (STAT3) signaling drives the development of HCC in obese mice without affecting NASH or fibrosis.³⁰ Consistently, STAT3 activation is enhanced in human HCC specimens.^{42,46} Given this critical role of STAT3 in HCC progression, we next determined the activation state of STAT3 in liver tumors by Western blot analysis. We found that phosphorylation of STAT3 was significantly lower in tumors from *Stk25* knockout mice when compared with wild-type controls (Figure 7D). Reduced STAT3 activation also was observed in liver sections from *Stk25*^{-/-} mice with both DEN- and CDAA-induced HCC by

Figure 5. (See previous page). Genetic ablation of STK25 in mice with DEN- or CDAA-induced HCC suppresses liver steatosis, inflammation, and fibrosis. (A) Representative liver sections stained with Picrosirius Red or Oil Red O, or processed for immunohistochemistry/immunofluorescence with anti-F4/80 (green), anti-Gr1 (Ly6C) (red), anti-collagen IV (green), anti-fibronectin (green), or α SMA (brown) antibodies; nuclei stained with DAPI (blue) in immunofluorescence images; counterstaining with hematoxylin in immunohistochemistry images. (B) Quantification of the staining. (C) Activity of plasma alanine aminotransferase (ALT). Scale bars: 50 μ m. Data are means \pm SEM from 8 to 10 mice per group. CD, chow diet; DAPI, 4',6-diamidino-2-phenylindole; HFD, high-fat diet; KO, knockout; ORO, Oil Red O; WT, wild-type. * $P < .05$, ** $P < .01$, and *** $P < .001$.



immunohistochemistry analysis using anti-phospho-STAT3 antibody (Figure 7E).

Together, these results indicate that STK25 deficiency in hepatocytes protects against tumor development with suppression of several molecular signaling pathways typically activated in aggressive human HCC.

Silencing of STK25 Inhibits Metastatic Capacity of HepG2 Cells

To further study the cell-autonomous mechanisms behind the tumor-mitigating effects of STK25 knockdown, we silenced this target in HepG2 hepatocellular carcinoma cells by a small interfering RNA (siRNA) approach. To mimic conditions in high-fat diet-fed mice and high-risk subjects, we subsequently exposed the cells for 48 hours to 100 $\mu\text{mol/L}$ oleic acid, known to efficiently induce steatosis in vitro (Figure 8A–C). Consistent with in vivo studies, STK25 knockdown in HepG2 cells significantly suppressed proliferation as shown by measuring the DNA synthesis rate as well as by staining for the proliferation markers Ki67 and PCNA (Figure 8D and E). We also found reduced apoptosis in STK25-deficient HepG2 cells as indicated by a decreased amount of cleaved CASP3-positive cells (Figure 8E). Migration/invasive capacity, quantified using a Transwell assay, also was suppressed significantly in HepG2 cells transfected with STK25 siRNA compared with nontargeting control siRNA (Figure 8F and G). Notably, we also detected lower proliferation, apoptosis, migration, and invasion in STK25-deficient HepG2 cells cultured without oleate supplementation; however, the effect of STK25 silencing was less pronounced in cells maintained under basal conditions (Figure 9A–D). Interestingly, reciprocal to STK25 knockdown, the overexpression of STK25 in HepG2 cells resulted in aggravated migration and invasion compared with the control cells transfected with the empty vector (Figure 10).

We further explored the expression levels of the markers of epithelial–mesenchymal transition (EMT) in HepG2 cells transfected with STK25 siRNA vs nontargeting control siRNA. We found that STK25 knockdown markedly reduced the levels of mesenchymal markers fibronectin and N-cadherin and, reciprocally, enhanced the abundance of epithelial marker E-cadherin (Figures 8E and 9B). Furthermore, the silencing of STK25 decreased the transcript levels of *Slug* and *Zeb1* (Figure 8H and 9E), which are the critical transcriptional factors regulating EMT of cancer cells.⁴⁷

Impaired liver autophagy caused by hepatitis C virus and hepatitis B virus infection and lipid toxicity is closely related to the pathogenesis of HCC.¹⁸ To this end, we found that the silencing of STK25 in HepG2 cells increased the ratio of LC3-

I to LC3-II approximately 2-fold, which is an indicator of enhanced autophagic flux (Figure 8I).

In all, these data indicate that STK25 antagonism suppresses the metastatic ability of HCC cells by inhibiting EMT and regulating autophagy.

Discussion

This study describes sterile 20-type kinase STK25 as a crucial promoter of hepatocellular carcinogenesis in the context of NASH. Using the DEN- and CDAA-induced models of HCC, we found that the livers from *Stk25* knockout mice showed markedly lower tumor burden compared with wild-type littermates, which was accompanied by reduced apoptosis and compensatory cell proliferation, as well as suppressed neoangiogenesis. Interestingly, in our study, the expression of AFP, YAP, GRP78, and EpCAM was attenuated in the livers from *Stk25*^{-/-} mice, supporting the importance of STK25 not only in the development of HCC but also in tumor progression.

Although mortality associated with most cancer types has decreased steadily over the past decades, both the incidence rate and deaths resulting from HCC have increased sharply.⁴⁸ Several anticancer drugs are available for HCC therapy today (regorafenib, sorafenib, and nivolumab have received regulatory approval both by European Medicines Agency and the Food and Drug Administration); however, the overall 5-year survival rate remains 30%–40%, and the recurrence rate is approximately 80% in patients with advanced HCC.⁴⁹ Importantly, the development of efficient anti-HCC therapies has been hampered by the poor understanding of molecular pathogenesis of HCC, and NASH-driven HCC in specific. Interestingly, several recent studies have emphasized the impact of lipid metabolism in HCC genesis with intrahepatocellular lipid accumulation inducing oxidative and ER stress as well as inflammation, which subsequently accelerate tumorigenesis.^{19,33,39} In this study, in both the DEN- and CDAA-induced models of HCC, the genetic ablation of STK25 protected the mice against hepatic lipid accumulation, which was accompanied by lower generation of ROS, suppressed ER stress, as well as reduced infiltration of inflammatory cells in the liver. Thus, STK25 is likely controlling HCC initiation and progression by altering the susceptibility to hepatic lipotoxicity.

We further show that depletion of STK25 suppresses hepatocellular tumor growth in mice through reduced apoptosis and lowered compensatory proliferation by a mechanism that involves the inactivation of STAT3, ERK1/2, and p38 signaling—the key pathways also implicated in human HCC.^{41,42,46} Because the subcellular localization of STK25 is strictly confined to intrahepatocellular lipid

Figure 6. (See previous page). STK25 disruption in mice protects against hepatic oxidative and ER stress in HCC. (A) Representative liver sections stained with dihydroethidium (DHE) (pink) or MitoTracker Red (red), or processed for immunofluorescence with anti-4-hydroxynonenal (anti-4-HNE) (green), anti-E06 (green), anti-KDEL (green), or anti-C/EBP homologous protein (anti-CHOP) (red) antibodies; nuclei stained with DAPI (blue). **(B)** Quantification of the staining. *Scale bars:* 50 μm ; except for MitoTracker Red staining: *scale bars:* 25 μm . Data are means \pm SEM from 6 to 10 mice per group. CD, chow diet; DAPI, 4',6-diamidino-2-phenylindole; HFD, high-fat diet; KO, knockout; WT, wild-type. ***P* < .01, ****P* < .001.

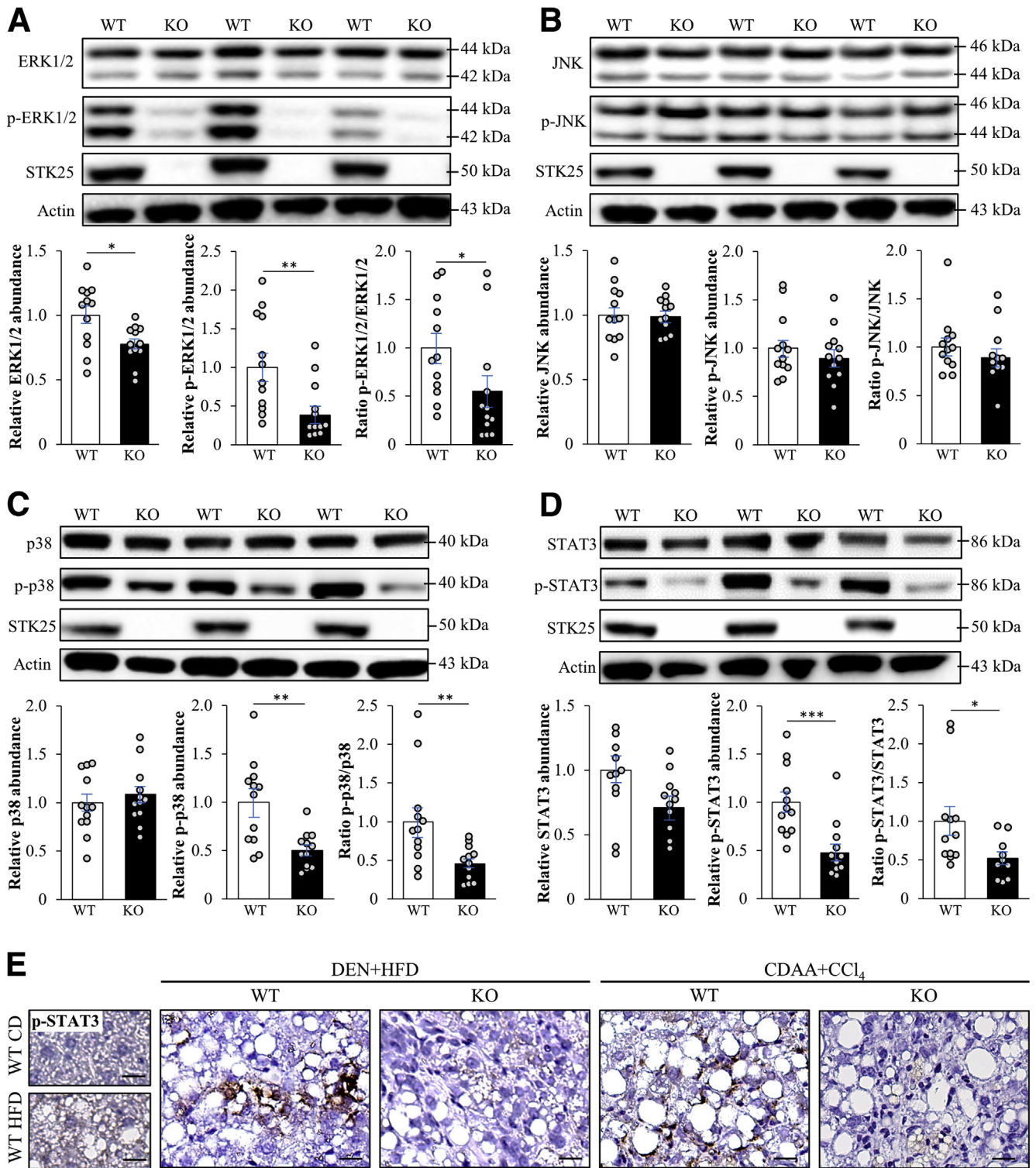
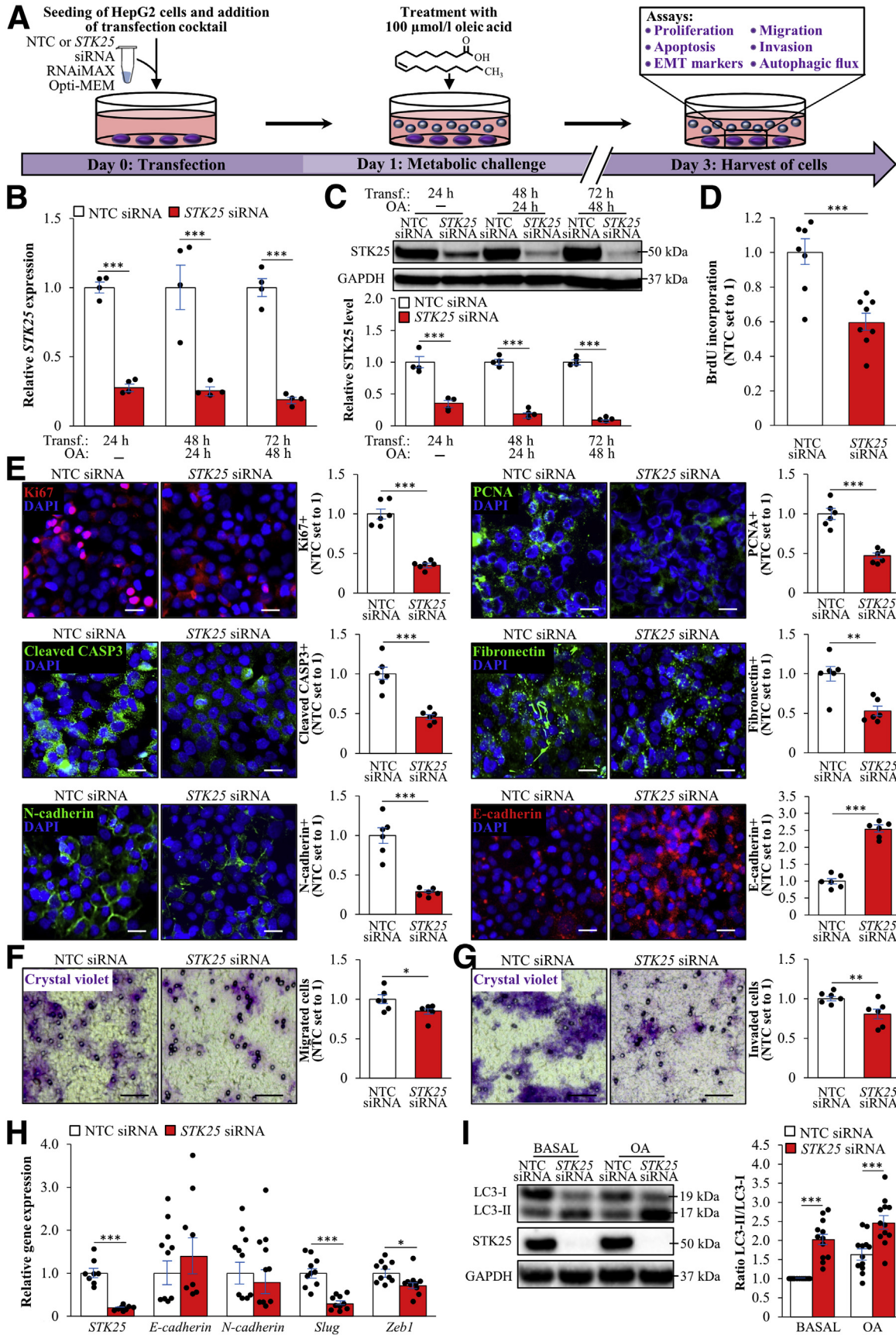


Figure 7. Genetic ablation of STK25 in a mouse model of DEN-induced HCC reduces the activation of key markers of tumorigenesis. (A–D) Lysates from liver tumors were analyzed by Western blot using antibodies specific for ERK1/2, phospho-ERK1/2 (Thr²⁰²/Tyr²⁰⁴), JNK, phospho-JNK (Thr¹⁸³/Tyr¹⁸⁵), p38, phospho-p38 (Thr¹⁸⁰/Tyr¹⁸²), STAT3, phospho-STAT3 (Thr⁷⁰⁵), and STK25. Protein levels were analyzed by densitometry; representative Western blots from 3 different mice per group are shown with actin used as a loading control. (E) Representative liver sections processed for immunohistochemistry with anti-phospho-STAT3 antibody; counterstaining with hematoxylin. Scale bars: 50 μ m. Data are means \pm SEM from 12 mice per group. CD, chow diet; HFD, high-fat diet; KO, knockout; WT, wild-type. * $P < .05$, ** $P < .01$, and *** $P < .001$.



droplets both in mouse and human liver cells,^{12,13,17} it is unlikely to directly phosphorylate these targets. Thus, the exact mechanisms by which STK25 alters STAT3, ERK1/2, and p38 activation remain elusive.

EMT has been widely recognized as a critical mechanism of cancer metastasis, an important reason for the poor prognosis of HCC patients.⁵⁰ To this end, it is significant that we detected suppressed mobility and invasiveness, as well as repressed expression of key molecular drivers of EMT, in STK25-deficient HepG2 cells, suggesting an additional mechanism underlying the lower HCC burden detected in *Stk25*^{-/-} mice in vivo.

A study by Lim et al⁵¹ recently identified STK25 as an activator of the Hippo signaling pathway by directly phosphorylating and activating LATS1/2. Hippo signaling normally acts to maintain tissue homeostasis and to suppress oncogenic co-activators YAP and TAZ. Consistent with this, STK25 deficiency was shown to lead to a moderate, but significant, increase in liver mass in mice at 6–12 months of age; however, liver carcinomas were not identified in any of the animals.⁵¹ In contrast, a recent report by Bae et al⁵² described STK25 as a suppressor of Hippo pathway activation by inhibiting mammalian sterile 20-like kinase (MST2). Thus, STK25 may have both positive and negative effects on this pathway, depending on the downstream signaling modality. Interestingly, messenger RNA expression analysis in hepatic tumors from more than 350 subjects also has identified STK25 as an unfavorable prognostic marker in human liver cancer because high expression of STK25 was associated with a lower 5-year survival rate compared with low expression.^{53,54} In line with these previous observations, in this study we found reduced hepatocyte proliferation and lower liver YAP abundance in HCC tumors from *Stk25* knockout mice.

Although the genetic deletion of STK25 suppressed hepatocellular carcinogenesis, it did not completely prevent the formation of HCC in mice. Notably, STK25 belongs to the GCKIII subfamily of sterile 20-type kinases together with 2 closely related kinases MST3 (also known as STK24) and MST4, which all are associated with lipid droplets in the liver and have similar functions regulating hepatocyte lipotoxicity and metabolic stress response in the context of obesity.^{12–14,17,55–57} It therefore is possible that antagonizing the activity of all 3 of these GCKIII kinases may promote the anti-HCC effect further.

In summary, we provide evidence that abrogation of STK25 hinders the acceleration of HCC development in mice in the context of NASH. The antitumor effect seen in mice by antagonizing the STK25 signaling pathway may open up new avenues for NASH-induced HCC treatment in human beings.

Materials and Methods

Animal Experiments

Stk25 knockout mice along with their wild-type littermates were generated and genotyped as reported earlier.²⁷ The male mice were weaned at 3 weeks of age and housed 3–5 per cage in a temperature-controlled (21°C) facility with a 12-hour light/dark cycle and ad libitum access to chow and water.

To induce HCC, a single intraperitoneal injection with DEN (25 mg/kg, N0258; Sigma-Aldrich, St. Louis, MO) was performed in 14-day-old *Stk25*^{-/-} and wild-type mice. Starting from 4 weeks after the DEN injection, mice were subjected to high-fat diet (60 kcal% fat, D12492; Research Diets, New Brunswick, NJ) feeding until 36 weeks of age.

HCC also was induced in another cohort of *Stk25*^{-/-} and wild-type mice by CDAA diet (30 kcal% fat-corn oil and palm oil, A18092701; Research Diets) feeding from the age of 6 to 43 weeks. During the CDAA diet-feeding period, mice were injected once weekly with a low-dose (0.2 µL/g of body weight) of CCl₄ (289116; Sigma-Aldrich) diluted (1:4 ratio) with corn oil (C8267; Sigma-Aldrich).²²

At age 36 weeks (for the DEN model) and 43 weeks (for the CDAA diet model), mice were killed after withholding food for 4 hours. To investigate the cell proliferation, mice were injected intraperitoneally with BrdU (100 mg/kg, B5002; Sigma-Aldrich) 2 hours before death.³² Blood was collected through heart puncture. Liver tissue was weighed, and each lobe of liver was photographed. Whole (tumor-bearing) liver tissue was collected for histologic and immunofluorescence/immunohistochemistry analysis as described later. Liver tumors also were isolated, snap frozen in liquid nitrogen, and stored at -80°C for Western blot analysis of protein expression.

The mice used in the study received humane care described by the National Institutes of Health (Bethesda, MD) recommendations outlined in the *Guide for the Care and Use of Laboratory Animals*. All the in vivo experiments

Figure 8. (See previous page). Silencing of STK25 in human HCC cells treated with oleic acid inhibits proliferation, mobility, and invasiveness. HepG2 cells were transfected with *STK25* siRNA or nontargeting control (NTC) siRNA and challenged with oleic acid for 48 hours. (A) Schematic illustration of the study design. (B and C) *STK25* (B) messenger RNA and (C) protein abundance. Protein levels were analyzed by densitometry; representative Western blots are shown with glyceraldehyde-3-phosphate dehydrogenase (GAPDH) used as a loading control. (D) The proliferation rate was assessed by measuring the DNA synthesis using a Biotrak cell proliferation enzyme-linked immunosorbent assay. (E) Representative images of cells processed for immunofluorescence with anti-Ki67 (red), anti-PCNA (green), anti-cleaved CASP3 (green), anti-fibronectin (green), anti-N-cadherin (green), or anti-E-cadherin (red) antibodies; nuclei stained with DAPI (blue). Quantification of the staining. (F and G) Representative images of (F) migrated and (G) invaded cells stained with crystal violet. Quantification of the staining. (H) Relative messenger RNA expression of selected EMT markers. (I) Cell lysates were analyzed by Western blot using antibodies specific for LC3 and *STK25*. Protein levels were analyzed by densitometry; representative Western blots are shown with GAPDH used as a loading control. (E) Scale bars: 15 µm; (F and G) scale bars: 50 µm. Data are means ± SEM from 4 to 10 wells per group. DAPI, 4',6-diamidino-2-phenylindole; OA, oleic acid; Transf, transfection. **P* < .05, ***P* < .01, and ****P* < .001.

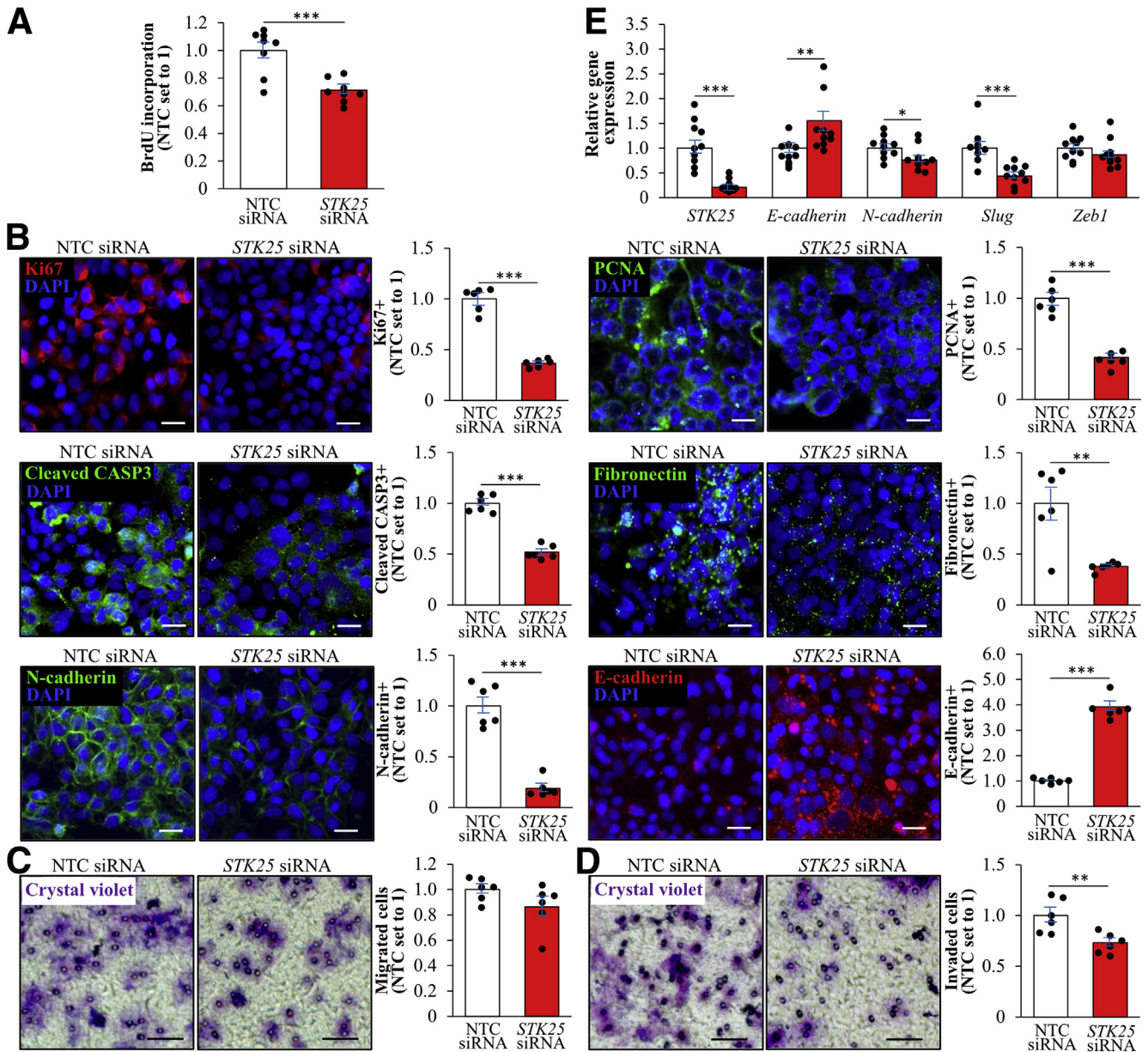


Figure 9. Silencing of STK25 in human HCC cells maintained under basal culture conditions inhibits proliferation, mobility, and invasiveness. HepG2 cells were transfected with *STK25* siRNA or nontargeting control (NTC) siRNA. (A) The proliferation rate was assessed by measuring the DNA synthesis using a Biotrak cell proliferation enzyme-linked immunosorbent assay. (B) Representative images of cells processed for immunofluorescence with anti-Ki67 (red), anti-PCNA (green), anti-cleaved CASP3 (green), anti-fibronectin (green), anti-N-cadherin (green), or anti-E-cadherin (red) antibodies; nuclei stained with DAPI (blue). Quantification of the staining. (C and D) Representative images of (C) migrated and (D) invaded cells stained with crystal violet. Quantification of the staining. (E) Relative messenger RNA expression of selected EMT markers. (B) Scale bars: 15 μ m; (C and D), scale bars: 50 μ m. Data are means \pm SEM from 6 to 10 wells per group. DAPI, 4',6-diamidino-2-phenylindole. * P < .05, ** P < .01, and *** P < .001.

were performed according to the protocols approved by the local Ethics Committee for Animal Studies at the Administrative Court of Appeals in Gothenburg, Sweden, following appropriate guidelines.

Liver Tumor Parameters

The photographs of liver lobes were used to measure the following tumor parameters: maximal tumor volume (the

volume of the largest visible HCC tumor found in each liver), total tumor volume (the sum of the volumes of all visible HCC tumors in each liver), and total tumor number.

Histologic and Immunofluorescence Analysis of Liver Sections

Liver tissue was fixed in 4% (vol/vol) phosphate-buffered formaldehyde (Histolab Products, Gothenburg,

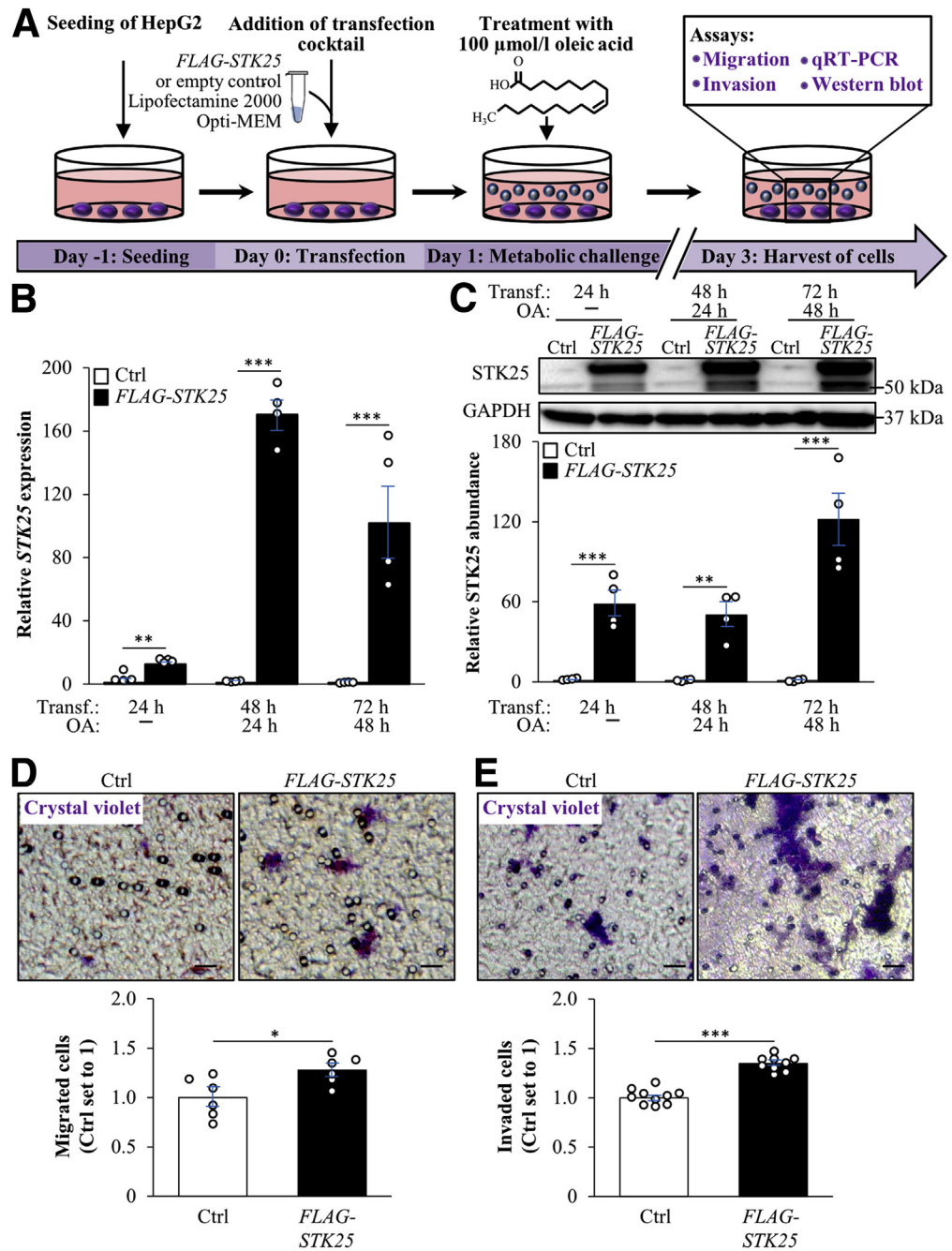


Figure 10. Overexpression of STK25 in human HCC cells increases mobility and invasiveness. HepG2 cells were transfected with *FLAG-STK25* or empty control plasmid and challenged with oleic acid for 48 hours. (A) Schematic illustration of the study design. (B and C) STK25 (B) messenger RNA and (C) protein abundance. Protein levels were analyzed by densitometry; representative Western blots are shown with glyceraldehyde-3-phosphate dehydrogenase (GAPDH) used as a loading control. (D and E) Representative images of (D) migrated and (E) invaded cells stained with crystal violet. Quantification of the staining. (D and E) Scale bars: 25 μm. Data are means ± SEM from 4 to 10 wells per group. Ctrl, control; OA, oleic acid; qRT-PCR, quantitative reverse-transcription polymerase chain reaction; Transf., transfection. **P* < .05, ***P* < .01, and ****P* < .001.

Sweden), embedded in paraffin, and sectioned. Paraffin sections were stained with H&E (Histolab Products) for morphologic analysis, with Picosirius Red (Histolab Products) for examination of the degree of fibrosis, or with dihydroethidium (Life Technologies, Grand Island, NY) to measure superoxide radical formation. Apoptotic cells were identified by using the horseradish-peroxidase-3,3'-diaminobenzidine tetra hydrochloride TUNEL Assay Kit (Abcam, Cambridge, UK).

Liver samples also were embedded in optimal cutting temperature mounting medium (Histolab Products) and frozen in liquid nitrogen, followed by cryosectioning.

Cryosections were stained with Oil Red O (Sigma-Aldrich) to access neutral lipids or MitoTracker Red (Thermo Fisher Scientific, Waltham, MA) for detection of respiring mitochondria. The labeled area was quantified in 6–8 randomly selected microscopic fields (×200; distributed over 3 nonconsecutive liver sections) per mouse using ImageJ software (version 1.47; National Institutes of Health).

For immunofluorescence or immunohistochemistry analysis, paraffin sections or cryosections were incubated with primary antibodies, followed by incubation with fluorescent dye-conjugated or biotinylated secondary antibodies (see Table 1 for antibody information). The total area

Table 1. List of Antibodies Used for Western Blot and Immunofluorescence Analysis

Type	Antibody name and catalog number	Working dilution	Company
Primary antibody	Anti-STK25 (25821-1-AP)	1:750	Proteintech (Chicago, IL)
	Anti-AFP (ab46799)	1:200	Abcam
	Anti-YAP (ab205270)	1:500	Abcam
	Anti-GRP78 (sc-166490)	1:250	Santa Cruz Biotechnology (Santa Cruz, CA)
	Anti-EpCAM (ab213500)	1:100	Abcam
	Anti-cleaved CASP3 (ab49822)	1:500	Abcam
	Anti-BrdU (ab6326)	1:100	Abcam
	Anti-Ki67 (14-5698-82)	1:200	Invitrogen (Waltham, MA)
	Anti-PCNA (MA5-11358)	1:200	Invitrogen
	Anti-CK-19 (ab15463)	1:100	Abcam
	Anti-CD31 (558736)	1:100	BD Biosciences (San Jose, CA)
	Anti-F4/80 (MCA497GA)	1:250	Bio-Rad
	Anti-Gr1 (Ly6C) (ab15627)	1:300	Abcam
	Anti-collagen IV (ab6586)	1:200	Abcam
	Anti-fibronectin (F3648)	1:300	Sigma-Aldrich
	Anti- α SMA (ab5694)	1:200	Abcam
	Anti-8-oxoguanine (ab62623)	1:500	Abcam
	Anti- γ H2Ax (ab81299)	1:250	Abcam
	Anti-4-HNE (ab46545)	1:500	Abcam
	Anti-E06 (330001S)	1:100	Avanti Polar Lipids, Inc (Alabaster, AL)
	Anti-KDEL (ab176333)	1:500	Abcam
	Anti-CHOP (MA1-250)	1:200	Invitrogen
	Anti-ERK1/2 (#9102)	1:1000	Cell Signaling Technology (Boston, MA)
	Anti-p-ERK1/2 (#9101)	1:1000	Cell Signaling Technology
	Anti-JNK (#9252)	1:1000	Cell Signaling Technology
	Anti-p-JNK (#4668)	1:500	Cell Signaling Technology
	Anti-p38 (#9212)	1:1000	Cell Signaling Technology
	Anti-p-p38 (#9211)	1:500	Cell Signaling Technology
	Anti-STAT3 (#4904)	1:1000	Cell Signaling Technology
	Anti-p-STAT3 (#9131)	1:500	Cell Signaling Technology
Anti-actin (#A2920)	1:500	Santa Cruz Biotechnology	
Anti-GAPDH (sc-47724)	1:1000	Santa Cruz Biotechnology	
Anti-N-cadherin (33-3900)	1:500	Invitrogen	
Anti-E-cadherin (14-3249-82)	1:200	Invitrogen	
Anti-LC3B (#2775)	1:1000	Cell Signaling Technology	
Secondary antibody	Alexa Fluor-488-labeled anti-mouse IgG (A21202)	1:500	Invitrogen
	Alexa Fluor-488-labeled anti-rabbit IgG (A11008)	1:500	Invitrogen
	Alexa Fluor-594-labeled anti-mouse IgG (A11005)	1:500	Invitrogen
	Alexa Fluor-594-labeled anti-rabbit IgG (A21207)	1:500	Invitrogen
	Alexa Fluor-594-labeled anti-rat IgG (A11007)	1:500	Invitrogen
	Anti-rat (biotin) (ab6733)	1:300	Abcam
	Anti-rabbit IgG (#7074)	1:1000	Cell Signaling Technology
Anti-mouse IgG (#7076)	1:1000	Cell Signaling Technology	

4-HNE, 4-hydroxynonenal; α SMA, α smooth muscle actin; CHOP, C/EBP homologous protein; CK-19, cytokeratin-19; GAPDH, glyceraldehyde-3-phosphate dehydrogenase.

labeled was quantified in 8 randomly selected microscopic fields ($\times 100$ or $\times 200$, distributed over 3 nonconsecutive liver sections) per mouse using ImageJ software.

Cell Culture, RNA Interference, and Transient Overexpression

HepG2 cells (hepatocellular carcinoma, human; American Type Culture Collection, Manassas, VA) were maintained in Dulbecco's modified Eagle medium (GlutaMAX

supplemented; Gibco, Paisley, UK) supplemented with 10% (vol/vol) fetal bovine serum and 1% (vol/vol) penicillin/streptomycin (Gibco). Cells were shown to be free of mycoplasma infection by the MycoAlert Mycoplasma Detection Kit (Lonza, Basel, Switzerland). Cells were transfected with STK25 siRNA (s20570; Ambion, Austin, TX) or scrambled siRNA (SIC001; Sigma-Aldrich) using Lipofectamine RNAi-Max and Opti-MEM (Thermo Fisher Scientific). Cells also were transfected with human FLAG-STK25 (GeneCopoeia, Rockville, MD) or an empty control plasmid using

Lipofectamine 2000 and Opti-MEM (Thermo Fisher Scientific). In most experiments described later, transfected cells were exposed to 100 $\mu\text{mol/L}$ oleic acid (Sigma-Aldrich) for 48 hours, which efficiently induces steatosis in vitro.

Cells were fixed in 4% (vol/vol) phosphate-buffered formaldehyde (Histolab Products) and then processed for immunofluorescence with anti-Ki67, anti-PCNA, anti-cleaved CASP3, anti-fibronectin, anti-E-cadherin, or anti-N-cadherin antibodies (see Table 1 for antibody information). The labeled area was quantified in 6–10 randomly selected microscopic fields ($\times 200$) per well using ImageJ software. Proliferation was measured using the BrdU-Labeling Assay Kit (Amersham Cell Proliferation Bio-trak enzyme-linked immunosorbent assay System; GE Healthcare, Chicago, IL). To assess migration, cells were added to the upper chambers of the Transwells with 8- μm pore size (Polycarbonate Cell Culture Inserts in Multi-Well Plates; Costar, Kennebunk, ME) and medium with 10% fetal bovine serum was added in the bottom chambers for a chemotactic gradient. After 24 hours, cells on the upper surface were removed using cotton swabs, and the cells on the bottom side of the membranes were fixed and stained with 0.1% crystal violet (Sigma-Aldrich). To determine the invasive capacity of cells, the Transwells were coated with Matrigel matrix (Corning, Bedford, MA) before the experiment.

Quantitative Real-Time Polymerase Chain Reaction

RNA was isolated from HepG2 cells with the EZNA Total RNA Kit (Omega Bio-Tek, Norcross, GA) according to the manufacturer's recommendations. Complementary DNA was synthesized using the High-Capacity Complementary DNA Reverse Transcription Kit (Applied Biosystems, Foster City, CA). Relative quantification was performed with the CFX Connect Real-Time System (Bio-Rad, Hercules, CA). Relative quantities of target transcripts were calculated after normalization of the data to the endogenous control, 18S ribosomal RNA (Applied Biosystems).

Western Blot

Western blot was performed as previously described⁵⁸ (see Table 1 for antibody information).

Statistical Analysis

Statistical significance between the groups was evaluated using the 2-sample Student *t* test with $P < .05$ considered statistically significant. All statistical analyses were performed using SPSS statistics (v24; IBM Corporation, Armonk, NY).

References

- Llovet JM, Zucman-Rossi J, Pikarsky E, Sangro B, Schwartz M, Sherman M, Gores G. Hepatocellular carcinoma. *Nat Rev Dis Primers* 2016;2:16018.
- Friedman SL. Focus. We've hit the iceberg – the threat of NASH-related HCC arrives. *J Hepatol* 2014;60:1–2.
- Dyson J, Jaques B, Chattopadhyay D, Lochan R, Graham J, Das D, Aslam T, Patanwala I, Gaggar S, Cole M, Sumpter K, Stewart S, Rose J, Hudson M, Manas D, Reeves HL. Hepatocellular cancer: the impact of obesity, type 2 diabetes and a multidisciplinary team. *J Hepatol* 2014;60:110–117.
- Anstee QM, Targher G, Day CP. Progression of NAFLD to diabetes mellitus, cardiovascular disease or cirrhosis. *Nat Rev Gastroenterol Hepatol* 2013;10:330–344.
- Sanyal A, Poklepovic A, Moyneur E, Barghout V. Population-based risk factors and resource utilization for HCC: US perspective. *Curr Med Res Opin* 2010;26:2183–2191.
- Chalasan N, Younossi Z, Lavine JE, Charlton M, Cusi K, Rinella M, Harrison SA, Brunt EM, Sanyal AJ. The diagnosis and management of nonalcoholic fatty liver disease: practice guidance from the American Association for the Study of Liver Diseases. *Hepatology* 2018;67:328–357.
- Schuster S, Cabrera D, Arrese M, Feldstein AE. Triggering and resolution of inflammation in NASH. *Nat Rev Gastroenterol Hepatol* 2018;15:349–364.
- Anstee QM, Reeves HL, Kotsiliti E, Govaere O, Heikenwalder M. From NASH to HCC: current concepts and future challenges. *Nat Rev Gastroenterol Hepatol* 2019;16:411–428.
- Wong RJ, Aguilar M, Cheung R, Perumpail RB, Harrison SA, Younossi ZM, Ahmed A. Nonalcoholic steatohepatitis is the second leading etiology of liver disease among adults awaiting liver transplantation in the United States. *Gastroenterology* 2015;148:547–555.
- Mittal S, Sada YH, El-Serag HB, Kanwal F, Duan Z, Temple S, May SB, Kramer JR, Richardson PA, Davila JA. Temporal trends of nonalcoholic fatty liver disease-related hepatocellular carcinoma in the veteran affairs population. *Clin Gastroenterol Hepatol* 2015;13:594–601.e1.
- Amrutkar M, Cansby E, Chursa U, Nunez-Duran E, Chanclon B, Stahlman M, Friden V, Manneras-Holm L, Wickman A, Smith U, Backhed F, Boren J, Howell BW, Mahlapuu M. Genetic disruption of protein kinase STK25 ameliorates metabolic defects in a diet-induced type 2 diabetes model. *Diabetes* 2015;64:2791–2804.
- Amrutkar M, Cansby E, Nunez-Duran E, Pirazzi C, Stahlman M, Stenfeldt E, Smith U, Boren J, Mahlapuu M. Protein kinase STK25 regulates hepatic lipid partitioning and progression of liver steatosis and NASH. *FASEB J* 2015;29:1564–1576.
- Amrutkar M, Chursa U, Kern M, Nunez-Duran E, Stahlman M, Sutt S, Boren J, Johansson BR, Marschall HU, Bluher M, Mahlapuu M. STK25 is a critical determinant in nonalcoholic steatohepatitis. *FASEB J* 2016;30:3628–3643.
- Amrutkar M, Kern M, Nunez-Duran E, Stahlman M, Cansby E, Chursa U, Stenfeldt E, Boren J, Bluher M, Mahlapuu M. Protein kinase STK25 controls lipid partitioning in hepatocytes and correlates with liver fat content in humans. *Diabetologia* 2016;59:341–353.
- Cansby E, Nunez-Duran E, Magnusson E, Amrutkar M, Booten SL, Kulkarni NM, Svensson LT, Boren J,

- Marschall HU, Aghajan M, Mahlapuu M. Targeted delivery of Stk25 antisense oligonucleotides to hepatocytes protects mice against nonalcoholic fatty liver disease. *Cell Mol Gastroenterol Hepatol* 2019;7:597–618.
16. Nunez-Duran E, Aghajan M, Amrutkar M, Sutt S, Cansby E, Booten SL, Watt A, Stahlman M, Stefan N, Haring HU, Staiger H, Boren J, Marschall HU, Mahlapuu M. Serine/threonine protein kinase 25 antisense oligonucleotide treatment reverses glucose intolerance, insulin resistance, and nonalcoholic fatty liver disease in mice. *Hepatol Commun* 2018;2:69–83.
 17. Nerstedt A, Kurhe Y, Cansby E, Caputo M, Gao L, Vorontsov E, Stahlman M, Nunez-Duran E, Boren J, Marschall HU, Mashek DG, Saunders DN, Sihlbom C, Hoy AJ, Mahlapuu M. Lipid droplet-associated kinase STK25 regulates peroxisomal activity and metabolic stress response in steatotic liver. *J Lipid Res* 2020; 61:178–191.
 18. Ueno T, Komatsu M. Autophagy in the liver: functions in health and disease. *Nat Rev Gastroenterol Hepatol* 2017; 14:170–184.
 19. Lebeaupin C, Vallee D, Hazari Y, Hetz C, Chevet E, Bailly-Maitre B. Endoplasmic reticulum stress signalling and the pathogenesis of non-alcoholic fatty liver disease. *J Hepatol* 2018;69:927–947.
 20. Verna L, Whysner J, Williams GM. N-nitrosodiethylamine mechanistic data and risk assessment: bioactivation, DNA-adduct formation, mutagenicity, and tumor initiation. *Pharmacol Ther* 1996;71:57–81.
 21. Brown ZJ, Heinrich B, Greten TF. Mouse models of hepatocellular carcinoma: an overview and highlights for immunotherapy research. *Nat Rev Gastroenterol Hepatol* 2018;15:536–554.
 22. De Minicis S, Agostinelli L, Rychlicki C, Sorice GP, Saccomanno S, Candelaresi C, Giaccari A, Trozzi L, Pierantonelli I, Mingarelli E, Marziani M, Muscogiuri G, Gaggini M, Benedetti A, Gastaldelli A, Guido M, Svegliati-Baroni G. HCC development is associated to peripheral insulin resistance in a mouse model of NASH. *PLoS One* 2014;9:e97136.
 23. Miura K, Kodama Y, Inokuchi S, Schnabl B, Aoyama T, Ohnishi H, Olefsky JM, Brenner DA, Seki E. Toll-like receptor 9 promotes steatohepatitis by induction of interleukin-1beta in mice. *Gastroenterology* 2010; 139:323–334.e7.
 24. Yang L, Miura K, Zhang B, Matsushita H, Yang YM, Liang S, Song J, Roh YS, Seki E. TRIF differentially regulates hepatic steatosis and inflammation/fibrosis in mice. *Cell Mol Gastroenterol Hepatol* 2017;3:469–483.
 25. Liu Y, Meyer C, Xu C, Weng H, Hellerbrand C, ten Dijke P, Dooley S. Animal models of chronic liver diseases. *Am J Physiol Gastrointest Liver Physiol* 2013; 304:G449–G468.
 26. Constandinou C, Henderson N, Iredale JP. Modeling liver fibrosis in rodents. *Methods Mol Med* 2005; 117:237–250.
 27. Matsuki T, Chen J, Howell BW. Acute inactivation of the serine-threonine kinase Stk25 disrupts neuronal migration. *Neural Dev* 2013;8:21.
 28. Liang S, Ma HY, Zhong Z, Dhar D, Liu X, Xu J, Koyama Y, Nishio T, Karin D, Karin G, McCubbin R, Zhang C, Hu R, Yang G, Chen L, Ganguly S, Lan T, Karin M, Kisseleva T, Brenner DA. NADPH oxidase 1 in liver macrophages promotes inflammation and tumor development in mice. *Gastroenterology* 2019;156:1156–1172.e6.
 29. Fitamant J, Kottakis F, Benhamouche S, Tian HS, Chuvin N, Parachoniak CA, Nagle JM, Perera RM, Lapouge M, Deshpande V, Zhu AX, Lai A, Min B, Hoshida Y, Avruch J, Sia D, Camprecios G, McClatchey AI, Llovet JM, Morrissey D, Raj L, Bardeesy N. YAP inhibition restores hepatocyte differentiation in advanced HCC, leading to tumor regression. *Cell Rep* 2015;10:1692–1707.
 30. Grohmann M, Wiede F, Dodd GT, Gurzov EN, Ooi GJ, Butt T, Rasmiena AA, Kaur S, Gulati T, Goh PK, Treloar AE, Archer S, Brown WA, Muller M, Watt MJ, Ohara O, McLean CA, Tiganis T. Obesity drives STAT-1-dependent NASH and STAT-3-dependent HCC. *Cell* 2018;175:1289–1306.e20.
 31. Naugler WE, Sakurai T, Kim S, Maeda S, Kim K, Elsharkawy AM, Karin M. Gender disparity in liver cancer due to sex differences in MyD88-dependent IL-6 production. *Science* 2007;317:121–124.
 32. Maeda S, Kamata H, Luo JL, Leffert H, Karin M. IKKbeta couples hepatocyte death to cytokine-driven compensatory proliferation that promotes chemical hepatocarcinogenesis. *Cell* 2005;121:977–990.
 33. Nakagawa H, Umemura A, Taniguchi K, Font-Burgada J, Dhar D, Ogata H, Zhong Z, Valasek MA, Seki E, Hidalgo J, Koike K, Kaufman RJ, Karin M. ER stress cooperates with hypernutrition to trigger TNF-dependent spontaneous HCC development. *Cancer Cell* 2014; 26:331–343.
 34. Sakurai T, He G, Matsuzawa A, Yu GY, Maeda S, Hardiman G, Karin M. Hepatocyte necrosis induced by oxidative stress and IL-1 alpha release mediate carcinogen-induced compensatory proliferation and liver tumorigenesis. *Cancer Cell* 2008;14:156–165.
 35. Bergmann J, Muller M, Baumann N, Reichert M, Heneweer C, Bolik J, Lucke K, Gruber S, Carambia A, Boretius S, Leuschner I, Becker T, Rabe B, Herkel J, Wunderlich FT, Mittrucker HW, Rose-John S, Schmidt-Arras D. IL-6 trans-signaling is essential for the development of hepatocellular carcinoma in mice. *Hepatology* 2017;65:89–103.
 36. Zhu AX, Duda DG, Sahani DV, Jain RK. HCC and angiogenesis: possible targets and future directions. *Nat Rev Clin Oncol* 2011;8:292–301.
 37. Tacke F, Zimmermann HW. Macrophage heterogeneity in liver injury and fibrosis. *J Hepatol* 2014;60:1090–1096.
 38. Hernandez-Gea V, Toffanin S, Friedman SL, Llovet JM. Role of the microenvironment in the pathogenesis and treatment of hepatocellular carcinoma. *Gastroenterology* 2013;144:512–527.
 39. Li W, Li Y, Siraj S, Jin H, Fan Y, Yang X, Huang X, Wang X, Wang J, Liu L, Du L, Chen Q. FUN14 domain-containing 1-mediated mitophagy suppresses hepatocarcinogenesis by inhibition of inflammasome activation in mice. *Hepatology* 2019;69:604–621.

40. Zuo Q, He J, Zhang S, Wang H, Jin G, Jin H, Cheng Z, Tao X, Yu C, Li B, Yang C, Wang S, Lv Y, Zhao F, Yao M, Cong W, Wang C, Qin W. PGC1alpha suppresses metastasis of HCC by inhibiting Warburg effect via PPARgamma-dependent WNT/beta-catenin/PDK1 axis. *Hepatology* 2021;73:644–660.
41. Min L, He B, Hui L. Mitogen-activated protein kinases in hepatocellular carcinoma development. *Semin Cancer Biol* 2011;21:10–20.
42. Calvisi DF, Ladu S, Gorden A, Farina M, Conner EA, Lee JS, Factor VM, Thorgeirsson SS. Ubiquitous activation of Ras and Jak/Stat pathways in human HCC. *Gastroenterology* 2006;130:1117–1128.
43. Li J, Huang Q, Long X, Zhang J, Huang X, Aa J, Yang H, Chen Z, Xing J. CD147 reprograms fatty acid metabolism in hepatocellular carcinoma cells through Akt/mTOR/SREBP1c and P38/PPARalpha pathways. *J Hepatol* 2015;63:1378–1389.
44. Luk ST, Ng KY, Zhou L, Tong M, Wong TL, Yu H, Lo CM, Man K, Guan XY, Lee TK, Ma S. Deficiency in embryonic stem cell marker reduced expression 1 activates mitogen-activated protein kinase kinase 6-dependent p38 mitogen-activated protein kinase signaling to drive hepatocarcinogenesis. *Hepatology* 2020;72:183–197.
45. Sakurai T, Maeda S, Chang L, Karin M. Loss of hepatic NF-kappa B activity enhances chemical hepatocarcinogenesis through sustained c-Jun N-terminal kinase 1 activation. *Proc Natl Acad Sci U S A* 2006;103:10544–10551.
46. He G, Yu GY, Temkin V, Ogata H, Kuntzen C, Sakurai T, Sieghart W, Peck-Radosavljevic M, Leffert HL, Karin M. Hepatocyte IKKbeta/NF-kappaB inhibits tumor promotion and progression by preventing oxidative stress-driven STAT3 activation. *Cancer Cell* 2010;17:286–297.
47. Nieto MA, Huang RY, Jackson RA, Thiery JP. Emt: 2016. *Cell* 2016;166:21–45.
48. Ryerson AB, Ehemann CR, Altekruze SF, Ward JW, Jemal A, Sherman RL, Henley SJ, Holtzman D, Lake A, Noone AM, Anderson RN, Ma J, Ly KN, Cronin KA, Penberthy L, Kohler BA. Annual report to the nation on the status of cancer, 1975–2012, featuring the increasing incidence of liver cancer. *Cancer* 2016;122:1312–1337.
49. Thomas MB, Zhu AX. Hepatocellular carcinoma: the need for progress. *J Clin Oncol* 2005;23:2892–2899.
50. Giannelli G, Koudelkova P, Dituri F, Mikulits W. Role of epithelial to mesenchymal transition in hepatocellular carcinoma. *J Hepatol* 2016;65:798–808.
51. Lim S, Hermance N, Mudianto T, Mustaly HM, Mauricio IPM, Vittoria MA, Quinton RJ, Howell BW, Cornils H, Manning AL, Ganem NJ. Identification of the kinase STK25 as an upstream activator of LATS signaling. *Nat Commun* 2019;10:1547.
52. Bae SJ, Ni L, Luo X. STK25 suppresses Hippo signaling by regulating SAV1-STRIPAK antagonism. *Elife* 2020;9:e54863.
53. Uhlen M, Fagerberg L, Hallstrom BM, Lindskog C, Oksvold P, Mardinoglu A, Sivertsson A, Kampf C, Sjostedt E, Asplund A, Olsson I, Edlund K, Lundberg E, Navani S, Szgyarto CA, Odeberg J, Djureinovic D, Takanen JO, Hober S, Alm T, Edqvist PH, Berling H, Tegel H, Mulder J, Rockberg J, Nilsson P, Schwenk JM, Hamsten M, von Feilitzen K, Forsberg M, Persson L, Johansson F, Zwahlen M, von Heijne G, Nielsen J, Ponten F. Proteomics. Tissue-based map of the human proteome. *Science* 2015;347:1260419.
54. <https://www.proteinatlas.org/ENSG00000115694-STK25/pathology/liver+cancer>. Accessed January 22, 2021.
55. Cansby E, Kulkarni NM, Magnusson E, Kurhe Y, Amrutkar M, Nerstedt A, Stahlman M, Sihlbom C, Marschall HU, Boren J, Bluhner M, Mahlapuu M. Protein kinase MST3 modulates lipid homeostasis in hepatocytes and correlates with nonalcoholic steatohepatitis in humans. *FASEB J* 2019;33:9974–9989.
56. Caputo M, Cansby E, Kumari S, Kurhe Y, Nair S, Stahlman M, Kulkarni NM, Boren J, Marschall HU, Bluhner M, Mahlapuu M. STE20-type protein kinase MST4 controls NAFLD progression by regulating lipid droplet dynamics and metabolic stress in hepatocytes. *Hepatology Commun* 2021;5:1183–1200.
57. Caputo M, Kurhe Y, Kumari S, Cansby E, Amrutkar M, Scandalis E, Booten SL, Ståhlman M, Boren J, Marschall HU, Aghajan M, Mahlapuu M. Silencing of STE20-type kinase MST3 in mice with antisense oligonucleotide treatment ameliorates diet-induced nonalcoholic fatty liver disease. *FASEB J* 2021;35:e21567.
58. Cansby E, Amrutkar M, Manneras Holm L, Nerstedt A, Reyahi A, Stenfeldt E, Boren J, Carlsson P, Smith U, Zierath JR, Mahlapuu M. Increased expression of STK25 leads to impaired glucose utilization and insulin sensitivity in mice challenged with a high-fat diet. *FASEB J* 2013;27:3660–3671.

Received April 22, 2021. Accepted September 28, 2021.

Correspondence

Address correspondence to: Margit Mahlapuu, PhD, Department of Chemistry and Molecular Biology, University of Gothenburg, Gothenburg, Sweden. e-mail: margit.mahlapuu@gu.se; fax: (46) 31-7863948.

CRediT Authorship Contributions

Yeshwant Kurhe (Funding acquisition: Supporting; Methodology: Lead; Writing – review & editing: Supporting)
 Mara Caputo (Methodology: Supporting; Writing – review & editing: Supporting)
 Emmelie Cansby (Methodology: Supporting; Writing – review & editing: Supporting)
 Ying Xia (Methodology: Supporting; Writing – review & editing: Supporting)
 Sima Kumari (Methodology: Supporting; Writing – review & editing: Supporting)
 Sumit Kumar Anand (Methodology: Supporting; Writing – review & editing: Supporting)
 Brian W. Howell (Writing – review & editing: Supporting)
 Hanns-Ulrich Marschall (Writing – review & editing: Supporting)
 Margit Mahlapuu, Prof. (Conceptualization: Lead; Funding acquisition: Lead; Project administration: Lead; Resources: Lead; Supervision: Lead; Writing – original draft: Lead; Writing – review & editing: Lead)

Conflicts of interest

The authors disclose no conflicts.

Funding

This work was supported by grants from the Swedish Research Council, the Swedish Cancer Society, the West Sweden Avtal om Läkarutbildning och Forskning Program, the Novo Nordisk Foundation, the Swedish Heart-Lung Foundation, the Swedish Diabetes Foundation, the Wenner-Gren Foundation, the Å. Wiberg Foundation, the Adlerbert Research Foundation, the I. Hultman Foundation, the F. Neubergh Foundation, the Prof. N. Svartz Foundation, the L. and J. Grönberg Foundation, the W. and M. Lundgren Foundation, and the I.-B. and A. Lundberg Research Foundation.